

VRHCF: CROSS-SOURCE POINT CLOUD REGISTRATION VIA VOXEL REPRESENTATION AND HIERARCHICAL CORRESPONDENCE FILTERING

Guiyu Zhao, Zewen Du, Zhentao Guo, Hongbin Ma*

National Key Lab of Autonomous Intelligent Unmanned Systems
School of Automation, Beijing Institute of Technology
*Corresponding author, Email: mathmh@bit.edu.cn

ABSTRACT

Addressing the challenges posed by the substantial gap in point cloud data collected from diverse sensors, achieving robust cross-source point cloud registration becomes a formidable task. In response, we present a novel framework for point cloud registration with broad applicability, suitable for both homologous and cross-source registration scenarios. To tackle the issues arising from different densities and distributions in cross-source point cloud data, we introduce a feature representation based on spherical voxels. Furthermore, addressing the challenge of numerous outliers and mismatches in cross-source registration, we propose a hierarchical correspondence filtering approach. This method progressively filters out mismatches, yielding a set of high-quality correspondences. Our method exhibits versatile applicability and excels in both traditional homologous registration and challenging cross-source registration scenarios. Specifically, in homologous registration using the 3DMatch dataset, we achieve the highest registration recall of 95.1% and an inlier ratio of 87.8%. In cross-source point cloud registration, our method attains the best RR on the 3DCSR dataset, demonstrating a 9.3 percentage points improvement. The code is available at <https://github.com/GuiyuZhao/VRHCF>.

Index Terms— Cross-source, point cloud registration, correspondence filtering

1. INTRODUCTION

Cross-source point cloud registration [1] involves aligning point cloud data from different sensors and methods, such as SFM and Kinect or Kinect and LiDAR, to the same coordinate system through rotation and translation. This process holds promising applications in various domains, including unmanned driving, remote sensing, and medicine. We can leverage cross-source point cloud registration to facilitate data calibration, thereby integrating the strengths of various sensors. This alignment facilitates multi-sensor fusion, opening avenues for advancements in various computer vision tasks.

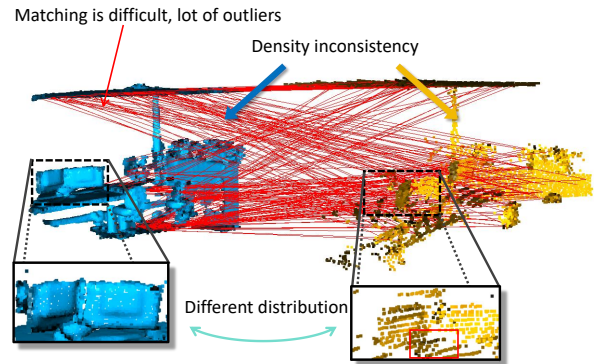


Fig. 1. Challenges in cross-source point cloud registration.

Cross-source point cloud registration [1] presents a formidable challenge within the broader task of point cloud registration. The inherent difficulty arises from two key challenges [1], as shown in Figure 1. **Firstly**, the diverse origins of point cloud data, stemming from different sensors, introduce significant disparities in cross-source datasets. Notably, the prominent issue is the density inconsistency and different distribution in point clouds, with LiDAR-generated point clouds exhibiting sparsity and line-like structures, in stark contrast to the dense nature of point clouds from depth cameras. This stark contrast complicates the task of learning similar features through feature metric learning. **Secondly**, the presence of numerous outliers in point clouds collected by distinct sensors, coupled with the intricate challenge of feature matching, results in a substantial number of mismatches in obtained correspondences. These dual challenges collectively pose substantial difficulties in achieving robust cross-source registration.

Currently, there is a lot of research focused on same-source registration [2, 3, 4, 5], yet the majority of these approaches exhibit bad performance in cross-source registration. Even SpinNet [3], known for its strong generalization, falls short in achieving generalization across different sources, limiting its applicability. Simultaneously, numerous cross-source registration algorithms [6, 7, 8] have been introduced in recent years, primarily relying on optimization meth-

ods. Unfortunately, although these methods achieve some improvement in cross-source registration, they perform poorly in unseen scenes and noisy scenes. In addition, most existing methods face challenges in effectively addressing the dual issues mentioned above, making it challenging to achieve robust cross-source registration.

Motivated by the challenges inherent in cross-source point cloud registration, we introduce a novel framework designed to address these difficulties, exhibiting good generalization ability across various scenes and excelling in both homologous and cross-source registration scenarios. **In response to the first challenge**, we present a feature representation based on spherical voxels. Departing from conventional downsampling methods [6] that risk feature loss, our approach leverages spherical voxels to achieve density-invariant representation without significant downsampling, thereby preventing the associated feature degradation. Feature refinement is subsequently conducted through the 3D cylindrical convolution network (3DCCN) backbone [3] to derive density-invariant feature descriptors. **For the second challenge**, we introduce hierarchical correspondence filtering—a refined and progressive mechanism for filtering false matches, resulting in a high-quality set of correspondences. Finally, using SVD [9], we achieve a more robust and accurate registration.

Our method demonstrates strong performance in both homologous and cross-source point cloud registration. Notably, in the cross-source 3DCSR *Kinect-sfm* benchmark, our approach outperforms the original method, achieving a substantial 9.3-percentage-point improvement at 93.8%, indicative of a more robust registration capability. On the challenging *Kinect-lidar* benchmark, our method demonstrates an improvement of 1.2 percentage points (pp) and 3.9 pp in RR and FMR, respectively. Additionally, in homologous point cloud registration, on the 3DMatch dataset, our method outshines other strong baselines, achieving the best performance with 95.1% RR and 87.8% IR. Our key contributions include:

- We introduce a novel registration framework that exhibits robust and precise cross-source and homologous registration, suitable for a diverse array of scenarios.
- A spherical voxel feature representation method is proposed to realize the feature representation with consistent density and avoid the feature loss caused by downsampling.
- hierarchical correspondence filtering is proposed to solve the problem of outliers and false matches in cross-source registration.

2. RELATED WORK

2.1. Cross-source point cloud registration

Cross-source point cloud registration [12, 1] has progressed at a slower pace compared to homologous point cloud regis-

tration due to the inherent challenges it presents. The difficulty in extracting similar features for corresponding points in cross-source registration has limited the development of feature-based methods [6]. Instead, previous mainstream approaches have primarily focused on optimization-based methods [13, 14, 7] and model-based methods [6, 8, 15]. Notably, GCC [7] has demonstrated superior performance in indoor cross-source point cloud registration, employing fuzzy clustering and ICP optimization [9]. The scarcity of cross-source data for training sets has hindered the development of learning-based registration methods. Addressing this limitation, SPEAL [16] has taken steps to construct a KITTI cross-source dataset for outdoor scenes through binocular estimation, enabling large-scale training.

2.2. Correspondence filtering

Due to challenges in cross-source data, feature matching is difficult, leading to the generation of numerous false correspondences. Therefore, correspondence filtering plays a pivotal role in cross-source registration. In recent years, correspondence filtering methods have experienced rapid development, categorized into learning-based methods [17, 18, 19, 20] and traditional geometric-based methods [21, 22, 23]. Learning-based methods [19, 20] often treat correspondence filtering as a classification problem, eliminating correspondences based on class assignment. For instance, 3DRegNet [20] incorporates CN-Net [24] into point cloud matching, employing a confidence-based classification module for correspondence filtering. PointDSC [19] enhances the effectiveness by incorporating geometric consistency into the network. Non-learning methods primarily rely on determining geometric consistency. SC2-PCR [22] introduces second-order spatial consistency for robust correspondence filtering, demonstrating its efficacy. MAC [23] achieves optimal results by introducing the maximal clique concept from graph theory.

3. METHOD

3.1. Spherical voxel-based feature representation

Due to the disparate origins of point cloud data acquired from various sensors, there exists substantial variation in the distribution and density of cross-source point cloud data. This discrepancy significantly impacts feature metric learning, impeding the accurate determination of correspondences and resulting in registration failures. To address this issue, a straightforward approach involves unifying the densities through extensive downsampling. However, this method has the drawback of compromising nearest neighbor information, ultimately leading to feature loss. In contrast to downsampling, our paper introduces a feature representation based on spherical voxels to tackle the density difference problem. The utilization of spherical voxelization and normalization achieves density-invariant feature representation, followed by

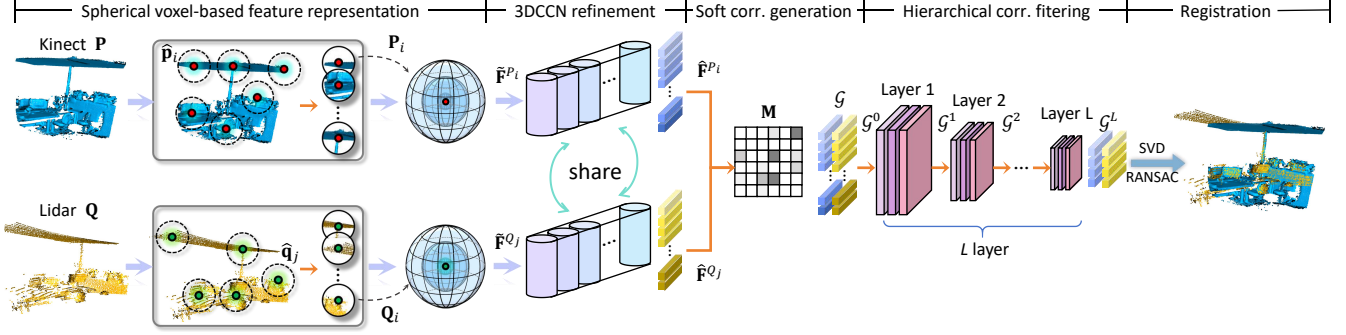


Fig. 2. Given cross-source point clouds \mathbf{P} and \mathbf{Q} , we first obtain local patches \mathbf{P}_i and \mathbf{Q}_j by FPS [10] and KNN search, and then complete the representation of initial features $\tilde{\mathbf{F}}^{\mathbf{P}_i}$ and $\tilde{\mathbf{F}}^{\mathbf{Q}_j}$ by spherical voxelization and multi-scale sphere normalization. Then, the features are refined by the 3DCCN backbone to obtain the features $\hat{\mathbf{F}}^{\mathbf{P}_i}$ and $\hat{\mathbf{F}}^{\mathbf{Q}_j}$. Soft correspondence generation is applied to loosely generate the initial correspondences \mathcal{G} , which are further filtered through hierarchical correspondence filtering to produce the final correspondence \mathcal{G}^L . The transformation \mathbf{T} is ultimately determined using SVD or RANSAC [11].

feature refinement through the 3DCCN backbone [3] to extract patch-based features.

Spherical voxelization. We employ spherical voxelization to mitigate the density difference between the cross-source point clouds \mathbf{P} and \mathbf{Q} . Inspired by the geographical coordinate system of the Earth (GCSE), we deviate from traditional cube voxelization and octree methods, and divide the patch-based sphere along three dimensions: longitude θ , latitude φ , and radius r , resulting in a voxel sphere and completing the initial feature representation. Notably, point cloud nearest neighbor searches involve k-nearest neighbor search and radius nearest neighbor search, with their search space approximating a sphere. Hence, our Spherical voxelization is better suited for representing nearest neighbor information than traditional cube voxels. Additionally, as we solely use spherical voxelization for feature representation, and the corresponding density-invariant features are normalized by the spheroid voxel without extensive downsampling, we incur less loss in neighbor information with the excessive downsampling.

In the original point cloud \mathbf{P} , we acquire k keypoints $\hat{\mathbf{P}}$ using the farthest point sampling (FPS) [10]. Subsequently, for each $\hat{\mathbf{p}}_i \in \hat{\mathbf{P}}$, a radius nearest neighbor search is conducted within the original point cloud \mathbf{P} . The nearest neighbor points are then aggregated to form the patch \mathbf{P}_i

$$\mathbf{P}_i = \left\{ \mathbf{p}_j | \mathbf{p}_j \in \text{RNN}(\hat{\mathbf{P}}; \hat{\mathbf{p}}_i, r) \right\} \quad (1)$$

where operator RNN represents a radius nearest neighbor search at $\hat{\mathbf{P}}$ with $\hat{\mathbf{p}}_i$ as the center and r as the radius. Next, we perform spherical voxelization on each patch \mathbf{P}_i . As illustrated in Figure 2, we establish our patch coordinate system following GCSE. The spherical patch is partitioned into N , M , and K regions in θ , φ , and r , respectively. Consequently, $N \times M \times K$ spherical voxels \mathbf{V}_{nmk}^i with $\hat{\mathbf{p}}_i$ as the center are generated. where n , m , and k represent the indices of voxels in the three dimensions. We characterize the initial

features $\mathbf{F}^{\mathbf{P}_i} \in \mathbb{R}^{N \times M \times K}$ by tallying the number of points $\mathbf{p}_i \in \mathbf{V}_{nmk}^i$ distributed in each small voxel \mathbf{V}_{nmk}^i . In the same way, we also extract patch-based feature $\mathbf{F}^{\mathbf{Q}_j}$ for point cloud \mathbf{Q} .

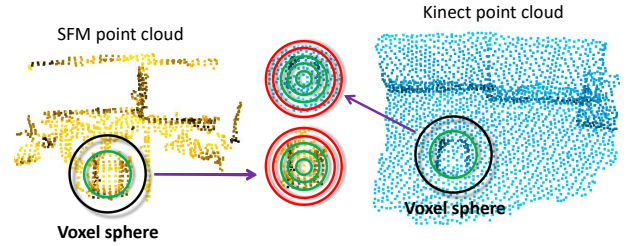


Fig. 3. The superiority of our normalization method where the green circle denotes the area where the point distribution of the two patches is the same, and the red indicates a difference. (For brevity, the split in the radius direction is plotted.)

Multi-scale sphere normalization. We then achieve density invariance of the features by quantitatively normalizing the voxel spheres. The simplest normalization involves directly dividing the number of points in each voxel \mathbf{V}_{nmk}^i of the sphere by the total number of points in the patch:

$$\tilde{\mathbf{F}}_{nmk}^{\mathbf{P}_i} = \frac{\mathbf{F}_{nmk}^{\mathbf{P}_i}}{\sum_{i=1}^N \sum_{j=1}^M \sum_{l=1}^K \mathbf{F}_{ijl}^{\mathbf{P}_i}} \quad (2)$$

However, this normalization method has limited effectiveness for cross-source data with significant differences in point cloud distribution. Figure 3 demonstrates that there are differences in the point distribution of the outer layer of the voxel sphere. Normalizing each layer's sphere separately can effectively mitigate the influence of distribution differences. Additionally, considering that 3DCCN [3] is convolved on the sphere of each layer, to better suit 3DCCN, we propose multi-scale sphere normalization. Through multi-scale sphere nor-

malization, we obtain the features of the k th layer after sphere normalization:

$$\tilde{\mathbf{F}}_{nmk}^{\mathcal{P}_i} = \frac{\mathbf{F}_{nmk}^{\mathcal{P}_i}}{\sum_{i=1}^N \sum_{j=1}^M \sum_{l=1}^k \mathbf{F}_{ijl}^{\mathcal{P}_i}}. \quad (3)$$

Using Eq. 3, we apply multi-scale normalization in the radial direction from the outer to the inner layers. In comparison to normalizing the entire sphere, our method provides an advantage: when the point cloud distribution differs in the outer layer of the multi-scale sphere (Figure 3), our normalization method does not affect the features of the inner layer. This enhances the robustness of our voxel representation.

Feature refinement. Although we construct the initial patch features through spherical voxelization and normalization, the inherent drawbacks [3] of handcrafted descriptors, make these initial features susceptible to noise. This sensitivity to noise becomes even more pronounced in cross-source point cloud registration, necessitating further refinement of features to enhance robustness. Drawing inspiration from SpinNet [3], we refine the patch features. In contrast to [3], we discard point-based layers [25, 3] and leverage spherical voxel occupancy to represent the initial features. We then refine the feature map using 3DCCN and obtain our final features $\hat{\mathbf{F}}^{\mathcal{P}_i} \in \mathbb{R}^{|\hat{\mathbf{P}}| \times d}$ through max-pooling:

$$\hat{\mathbf{F}}^{\mathcal{P}_i} = \mathcal{M}(3\text{DCCN}(\tilde{\mathbf{F}}^{\mathcal{P}_i})), \tilde{\mathbf{F}}_{nmk}^{\mathcal{P}_i} \in \tilde{\mathbf{F}}^{\mathcal{P}_i} \quad (4)$$

where $\mathcal{M}(\cdot)$ is max-pooling operator and $3\text{DCCN}(\cdot)$ denotes performing the 3DCCN operation.

3.2. Hierarchical correspondence filtering

In the task of cross-source point cloud registration, the inherent distribution differences between point clouds pose a challenge [1] for matching similar features at corresponding points. Consequently, the feature matching results exhibit a high prevalence of false correspondences. To address this issue, filtering the correspondences becomes crucial. Although a straightforward solution to reduce the number of mismatches is to employ mutual nearest neighbor (MNN) matching [26], this method is not suitable for the cross-source point cloud registration task. The stringent filtering conditions of MNN matching [26] may erroneously eliminate the correct correspondences, ultimately leading to registration failure. To overcome this challenge, we propose a more robust and efficient correspondence filtering method.

Soft correspondence generation. In order to capture all the correct correspondences as far as possible, we first conduct soft feature matching. This involves calculating the distances between keypoint $\hat{\mathbf{P}}$ and $\hat{\mathbf{Q}}$ in the feature space, yielding the matching distance matrix $\mathbf{S} \in \mathbb{R}^{|\hat{\mathbf{P}}| \times |\hat{\mathbf{Q}}|}$

$$\mathbf{S}_{i,j} = \frac{\hat{\mathbf{F}}^{\mathcal{P}_i}}{(\sum_{k=1}^d (\hat{\mathbf{F}}_k^{\mathcal{P}_i})^2)^{1/2}} \cdot \frac{\hat{\mathbf{F}}^{\mathcal{Q}_j}}{(\sum_{k=1}^d (\hat{\mathbf{F}}_k^{\mathcal{Q}_j})^2)^{1/2}} \quad (5)$$

where d is the dimension of the feature and $\hat{\mathbf{F}}_k^{\mathcal{Q}_j}$ denotes the k th value of feature $\hat{\mathbf{F}}^{\mathcal{Q}_j}$. The matrix \mathbf{S} undergoes softmax operations applied to both row and column [27], resulting in a soft assignment matrix \mathbf{M}

$$\mathbf{M}_{i,j} = \text{Softmax}(\mathbf{S}_{n,j})_i \text{Softmax}(\mathbf{S}_{i,m})_j \quad (6)$$

where Softmax denotes the softmax operation. Utilizing the score matrix \mathbf{M} , we apply the Top- k method to perform the element-wise selection, yielding the initial correspondence \mathcal{G}

$$\mathcal{G} = \{(\hat{\mathbf{p}}_n, \hat{\mathbf{q}}_m) \mid (n, m) \in \text{Topk}_{i,j}(\mathbf{M}_{i,j})\} \quad (7)$$

Hierarchical correspondence filtering. In cross-source datasets, diverse noise arises from distinct sensors [1]. Simultaneously, correspondences are generated through soft matching, leading to a substantial proportion of outliers. This abundance of outliers poses significant challenges in transformation estimation, rendering the robust estimator RANSAC [11] ineffective. Consequently, additional filtration of false correspondences is imperative for achieving robust registration. Drawing inspiration from SC^2 -PCR [22], we leverage the consistency of correct correspondences to filter the correspondences. Aiming at the problem that the single-stage method based on second-order consistency [22] fails under a high proportion of outliers, we introduce a progressive, hierarchical correspondence filtering method.

Taking layer l as an example, the input correspondences of this filtering layer is the output of the previous layer \mathcal{G}^{l-1} , where $l \in 1, 2, \dots, L$ and $\mathcal{G}^0 = \mathcal{G}$. In Euclidean space, the consistency distance $d_{i,j}^l$ between correspondences \mathcal{G}_i^{l-1} and \mathcal{G}_j^{l-1} at layer l is calculated:

$$d_{i,j}^l = \left| \|\hat{\mathbf{p}}_i^{l-1} - \hat{\mathbf{p}}_j^{l-1}\|_2 - \|\hat{\mathbf{q}}_i^{l-1} - \hat{\mathbf{q}}_j^{l-1}\|_2 \right| \quad (8)$$

where $\mathcal{G}_i^{l-1} = (\hat{\mathbf{p}}_i^{l-1}, \hat{\mathbf{q}}_i^{l-1}) \in \mathcal{G}^{l-1}$. And the consistency score is defined as $s_{i,j}^l = \mathbf{1}(d_{i,j}^l \leq \sigma_d)$ where σ_d is a distance threshold. Based on this consistency score, the second-order consistency score $ss_{i,j}^l$ between every two pairs of correspondences is determined:

$$ss_{i,j}^l = s_{i,j}^l \sum_{k=1}^{N^l} s_{i,k}^l \cdot s_{k,j}^l \quad (9)$$

where N^{l-1} is the number of correspondences \mathcal{G}_i^{l-1} . Employing the second-order consistency score, 80% of the correspondences are selected using the Top- k (percentage) method as the output correspondences of l th layer

$$\mathcal{G}^l = \{\mathcal{G}_i^{l-1} \mid i \in \text{Topk-p}_x(\sum_{y=1}^{N^{l-1}} ss_{x,y}^l)\} \quad (10)$$

where $\text{Topk-p}_x(\cdot)$ represents performing Top- k (percentage) operation along the x axis. As illustrated in Figure 2, our final correspondences \mathcal{G}^L are obtained through a hierarchical

correspondence filtering process. This progressive multi-step outlier removal method can robustly retain more correct correspondences while removing outliers, compared to the one-stage outlier removal methods. Finally, utilizing the obtained correspondences \mathcal{G}^L , we estimate transformation $\mathbf{T}\{\mathbf{R}, \mathbf{t}\}$ through weighted SVD or RANSAC [11], ensuring a robust and accurate cross-source registration.

4. EXPERIMENTS

We evaluate the performance of our method on both the cross-source dataset 3DCSR (Sec. 4.1) and the homologous dataset 3DMatch (Sec. 4.2). In addition, we also set up ablation experiments to verify the effectiveness of each of our modules (Sec. 4.3). The training for 3DMatch followed the experimental setup of SpinNet [3]. However, for 3DCSR, where there is no extensive training set available, we address the density variations between cross-source datasets by downsampling the source point clouds from 3DMatch. Implementation details and runtime analysis are provided in Appx. A and C.

4.1. Evaluation on cross-source dataset

Dataset. The 3DCSR dataset comprises 202 indoor scenes encompassing two cross-source types. These include point clouds transitioning from those collected by Kinect to those generated by Structure from Motion (SfM), and from Kinect to LiDAR-collected point clouds. The dataset consists of 37 scenes for *Kinect-sfm* and 165 scenes for *Kinect-Lidar*, both of which are classified as easy and challenging.

Metrics. Following [7], we utilize translation error (TE), rotation error (RE), and registration recall (RR) to evaluate our method. And following [2], we assess correspondence results using inlier ratio (IR) and feature matching recall (FMR). Detailed metrics are explained in Appx. B.

Results. We divide the experiments into two parts based on the source categories: *Kinect-sfm* and *Kinect-lidar*. Our method is compared with cross-source registration methods ICP [9], GICP [28], JRMPC [6], GCTR [8], GCC [7] and homologous registration methods SpinNet [3], Predator [4], CoFiNet [29], GeoTrans [2]. The results are presented in Table 1. Our method outperforms in 3DCSR *Kinect-sfm*, with a 9.3 percentage point (pp) and 35.7 pp increase in RR and IR compared to the SOTA [3]. In extremely challenging *Kinect-lidar* scenarios, our method, like others [7, 2], exhibits a low level in RR. Nevertheless, in comparison with previous methods [7, 2], ours shows great improvements in all metrics, particularly with a 3.9 pp increase in FMR. The visualization of qualitative results on 3DCSR is shown in Figure 4.

4.2. Evaluation on homologous dataset

Dataset. The 3DMatch dataset is an indoor dataset reconstructed from RGBD images, comprising a total of 62 scenes.

Method	RR(↑)	IR(↑)	FMR(↑)	RRE(↓)	RTE(↓)
<i>Kinect-sfm</i>					
ICP [9]	18.8	-	-	2.79	0.08
GICP [28]	12.5	-	-	1.90	0.03
JRMPC [6]	0	3.3	14.8	-	-
GCTR [8]	15.2	10.9	46.8	2.99	0.10
GCC [7]	81.3	-	-	2.09	0.06
SpinNet [3]	<u>84.5</u>	<u>54.8</u>	<u>93.8</u>	2.64	0.08
Predator [4]	71.8	31.8	81.3	3.93	0.11
CoFiNet [29]	37.5	25.3	90.6	4.19	0.10
GeoTransformer [2]	84.4	40.2	90.6	<u>1.95</u>	<u>0.06</u>
VRHCF (<i>ours</i>)	93.8	90.3	96.8	2.06	<u>0.06</u>
<i>Kinect-lidar</i>					
ICP [9]	1.3	-	-	7.86	0.24
GICP [28]	0.6	-	-	12.8	0.24
JRMPC [6]	0	0.5	3.1	-	-
GCTR [8]	0	0.1	2.1	-	-
GCC [7]	3.1	-	-	<u>3.64</u>	<u>0.15</u>
SpinNet [3]	5.2	1.2	7.1	6.93	0.15
Predator [4]	5.2	0.5	1.3	4.63	0.21
CoFiNet [29]	5.2	1.2	7.1	4.65	0.15
GeoTransformer [2]	<u>9.1</u>	<u>3.4</u>	<u>9.7</u>	4.60	0.17
VRHCF (<i>ours</i>)	10.3	6.4	13.6	3.41	0.13

Table 1. Quantitative results on 3DCSR.

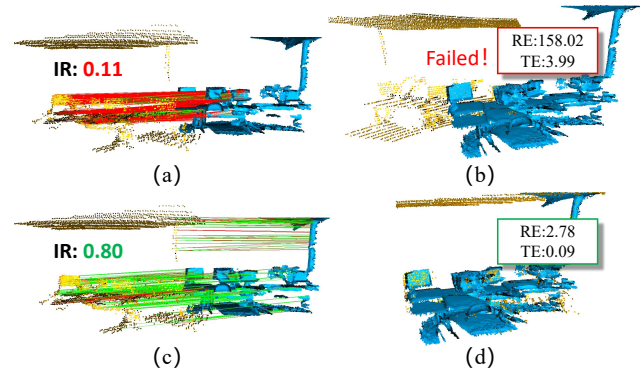


Fig. 4. Qualitative results. The correct correspondences are denoted by the green lines, while the red lines indicate errors.

Among these, 58 scenes are allocated to the training set, 8 scenes for the validation set, and 8 scenes for the test set. According to [4], the dataset has two benchmarks, distinguished by the overlap (>30% or not): 3DMatch and 3DLoMatch.

Metrics. Similar to the 3DCSR experiment, we use IR, FMR, and RR to evaluate the performance. However, when calculating RR for homologous registration, we consider the registration with RMSE < 0.2m as a successful registration.

Results. Our method is compared with Predator [4], SphereNet [30], CoFiNet [29], GeoTrans [2] and RoITr [31]. The experimental results are presented in Table 2. Our method and GeoTrans employ SVD for transformation estimation, while other methods utilize RANSAC [11]. Table 2 illustrates that our method attains superior results on 3DMatch, boasting an RR as high as 95.1%, with a 3.2 pp increase compared with [2]. In addition, our method significantly outperforms in correspondence results, achieving an IR

of 87.9%, a 5.2 pp improvement over [31]. Furthermore, our method also excels in both RR and IR on 3DLoMatch, showcasing it is robust to low overlap. In addition, our method is also robust to the number of sampling points and achieves the best results for different numbers of sampling points. However, our method in FMR is inferior to RoITr and GeoTrans. Because, in some scenarios where the original IR is very low (but $IR \geq 5\%$), due to the influence of a large number of anomalies, our HCF module incorrectly filters out the correct correspondence, ultimately resulting in $IR < 5\%$.

In summary, our method demonstrates effectiveness for both cross-source and same-source scenarios.

# Samples	3DMatch					3DLoMatch				
	5000	2500	1000	500	250	5000	2500	1000	500	250
<i>Feature Matching Recall (%)</i> ↑										
Predator [4]	96.6	96.6	96.5	96.3	96.5	78.6	77.4	76.3	75.7	75.3
CoFiNet [29]	<u>98.1</u>	98.3	<u>98.1</u>	98.2	98.3	83.1	83.5	83.3	83.1	82.6
GeoTransformer [2]	97.9	97.9	97.9	97.9	97.6	<u>88.3</u>	<u>88.6</u>	<u>88.8</u>	<u>88.6</u>	<u>88.3</u>
SphereNet [30]	98.2	98.3	98.2	97.3	95.8	79.1	78.5	77.3	74.1	68.4
RoITr [31]	98.0	<u>98.0</u>	97.9	<u>98.0</u>	<u>97.9</u>	89.6	89.6	89.5	89.4	89.3
VRHCF (ours)	96.7	96.9	96.9	96.9	96.0	82.1	82.1	82.0	82.0	81.6
<i>Inlier Ratio (%)</i> ↑										
Predator [4]	58.0	58.4	57.1	54.1	49.3	26.7	28.1	28.3	27.5	25.8
CoFiNet [29]	49.8	51.2	51.9	52.2	52.2	24.4	25.9	26.7	26.8	26.9
GeoTransformer [2]	71.9	75.2	76.0	82.2	<u>85.1</u>	43.5	45.3	46.2	52.9	57.7
SphereNet [30]	54.2	54.6	54.3	48.9	44.2	24.2	24.8	25.0	22.7	19.2
RoITr [31]	<u>82.6</u>	<u>82.8</u>	83.0	<u>83.0</u>	83.0	<u>54.3</u>	<u>54.6</u>	<u>55.1</u>	<u>55.2</u>	<u>55.3</u>
VRHCF(ours)	87.8	87.6	87.6	87.6	87.5	62.6	62.6	62.0	61.7	61.9
<i>Registration Recall (%)</i> ↑										
Predator [4]	89.0	89.9	90.6	88.5	86.6	59.8	61.2	62.4	60.8	58.1
CoFiNet [29]	89.1	88.9	88.4	87.4	87.0	67.5	66.2	64.2	63.1	61.0
GeoTransformer [2]	<u>92.0</u>	<u>91.8</u>	<u>91.8</u>	<u>91.4</u>	<u>91.2</u>	<u>75.0</u>	<u>74.8</u>	74.2	74.1	73.5
SphereNet [30]	91.2	90.3	88.8	86.2	77.7	60.0	59.6	53.9	45.5	32.4
RoITr [31]	91.9	91.7	<u>91.8</u>	<u>91.4</u>	91.0	74.7	<u>74.8</u>	<u>74.8</u>	<u>74.2</u>	<u>73.6</u>
VRHCF (ours)	95.1	94.6	94.9	94.9	94.3	76.8	76.8	76.7	76.7	76.4

Table 2. Quantitative results on 3DMatch and 3DLoMatch.

4.3. Ablation study

We conduct ablation experiments to assess the effectiveness of each module. We present a complete model and four ablation models, with the experimental results detailed in Table 3. **Multi-scale sphere normalization (MSN)**. The model without MSN experiences a notable performance decline on the 3DCSR dataset, as depicted in (1) and (2) of Table 3. This emphasizes the significance of our MSN module, which addresses the density inconsistency issue and is effective for cross-source registration.

Spherical voxelization (SV). As depicted in (1) and (3), the performance of the model without SV further decreases on both datasets. Because SV plays a pivotal role in feature representation and contributes to achieving robust registration.

Soft correspondence generation (SCG) or mutual nearest neighbor (MNN). Shown in (1) and (4), the model with SCG outperforms the model with MNN on 3DCSR, while its performance degrades on 3DMatch. This discrepancy arises

No.	SV	MSN	SCG	MNN	HCF	3DCSR			3DMatch		
						RR(↑)	IR(↓)	FMR(↓)	RR(↑)	IR(↓)	FMR(↓)
1)	✓	✓	✓		✓	93.8	90.3	96.8	95.1	87.8	96.7
2)	✓		✓		✓	87.8	86.8	90.1	94.9	87.4	96.3
3)			✓		✓	84.5	82.4	93.8	93.0	85.2	96.3
4)	✓	✓		✓	✓	84.5	89.7	87.8	95.1	88.2	96.2
5)	✓	✓	✓			90.1	57.4	90.6	91.0	52.1	97.9

Table 3. Ablation results on 3DCSR and 3DMatch.

while its performance degrades on 3DMatch. This discrepancy arises because the SCG module is more suitable for scenarios with numerous false correspondences, demonstrating superior performance in cross-source registration.

Hierarchical correspondence filtering (HCF). Illustrated in (1) and (5), the incorporation of the HCF module significantly enhances the performance of our method compared to the case without the HCF module. It plays a crucial role in achieving robust and accurate registration.

5. CONCLUSION

This paper introduces a novel framework for cross-source point cloud registration, aiming to realize robust and accurate registration. To address challenges arising from inconsistent density and distribution differences in cross-source data, we propose a spherical voxel-based feature representation for feature extraction. Additionally, to tackle difficulties in matching cross-source point features and mitigating the impact of numerous mismatches, we present soft correspondence generation and hierarchical correspondence filtering. These methods aim to enhance the quality of correspondences, leading to more robust registration. In the future, an indoor cross-source point cloud dataset will be collected and produced for large-scale training.

6. REFERENCES

- [1] Xiaoshui Huang, Guofeng Mei, and Jian Zhang, “Cross-source point cloud registration: Challenges, progress and prospects,” *Neurocomputing*, p. 126383, 2023.
- [2] Zheng Qin, Hao Yu, Changjian Wang, Yulan Guo, Yuxing Peng, and Kai Xu, “Geometric transformer for fast and robust point cloud registration,” in *CVPR*, 2022, pp. 11143–11152.
- [3] Sheng Ao, Qingyong Hu, Bo Yang, Andrew Markham, and Yulan Guo, “Spinnet: Learning a general surface descriptor for 3d point cloud registration,” in *CVPR*, 2021, pp. 11753–11762.
- [4] Shengyu Huang, Zan Gojcic, Mikhail Usvyatsov, Andreas Wieser, and Konrad Schindler, “Predator: Registration of 3d point clouds with low overlap,” in *CVPR*, 2021, pp. 4267–4276.
- [5] Yiheng Li, Canhui Tang, Runzhao Yao, Aixue Ye, Feng Wen, and Shaoyi Du, “Hybridpoint: Point cloud regis-

- tration based on hybrid point sampling and matching,” in *ICME*, 2023, pp. 2021–2026.
- [6] Xiaoshui Huang, Jian Zhang, Qiang Wu, Lixin Fan, and Chun Yuan, “A coarse-to-fine algorithm for matching and registration in 3d cross-source point clouds,” *IEEE TCSVT*, vol. 28, no. 10, pp. 2965–2977, 2017.
- [7] Mingyang Zhao, Xiaoshui Huang, Jingen Jiang, Luntian Mou, Dong-Ming Yan, and Lei Ma, “Accurate registration of cross-modality geometry via consistent clustering,” *IEEE TVCG*, 2023.
- [8] Xiaoshui Huang, Lixin Fan, Qiang Wu, Jian Zhang, and Chun Yuan, “Fast registration for cross-source point clouds by using weak regional affinity and pixel-wise refinement,” in *ICME*, 2019, pp. 1552–1557.
- [9] P.J. Besl and Neil D. McKay, “A method for registration of 3-d shapes,” *IEEE TPAMI*, vol. 14, no. 2, pp. 239–256, 1992.
- [10] Charles R Qi, Hao Su, Kaichun Mo, and Leonidas J Guibas, “Pointnet: Deep learning on point sets for 3d classification and segmentation,” in *CVPR*, 2017, pp. 652–660.
- [11] Martin A Fischler and Robert C Bolles, “Random sample consensus: a paradigm for model fitting with applications to image analysis and automated cartography,” *Communications of the ACM*, vol. 24, no. 6, pp. 381–395, 1981.
- [12] Xiaoshui Huang, Guofeng Mei, Jian Zhang, and Rana Abbas, “A comprehensive survey on point cloud registration,” *arXiv preprint arXiv:2103.02690*, 2021.
- [13] Jiaolong Yang, Hongdong Li, and Yunde Jia, “Goi-cp: Solving 3d registration efficiently and globally optimally,” in *ICCV*, 2013, pp. 1457–1464.
- [14] M Lamine Tazir, Tawsif Gokhool, Paul Checchin, Laurent Malaterre, and Laurent Trassoudaine, “Cicp: Cluster iterative closest point for sparse–dense point cloud registration,” *Rob. Auton. Syst.*, vol. 108, pp. 66–86, 2018.
- [15] Xiao Ling and Rongjun Qin, “A graph-matching approach for cross-view registration of over-view and street-view based point clouds,” *ISPRS J. Photogramm.*, vol. 185, pp. 2–15, 2022.
- [16] Kezheng Xiong, Maoji Zheng, Qingshan Xu, Chenglu Wen, Siqi Shen, and Cheng Wang, “Speal: Skeletal prior embedded attention learning for cross-source point cloud registration,” *arXiv preprint arXiv:2312.08664*, 2023.
- [17] Junha Lee, Seungwook Kim, Minsu Cho, and Jaesik Park, “Deep hough voting for robust global registration,” in *ICCV*, 2021, pp. 15994–16003.
- [18] Christopher Choy, Wei Dong, and Vladlen Koltun, “Deep global registration,” in *CVPR*, 2020, pp. 2514–2523.
- [19] Xuyang Bai, Zixin Luo, Lei Zhou, Hongkai Chen, Lei Li, Zeyu Hu, Hongbo Fu, and Chiew-Lan Tai, “Pointdsc: Robust point cloud registration using deep spatial consistency,” in *CVPR*, 2021, pp. 15859–15869.
- [20] G. Dias Pais, Srikumar Ramalingam, Venu Madhav Govindu, Jacinto C. Nascimento, Rama Chellappa, and Pedro Miraldo, “3dregnet: A deep neural network for 3d point registration,” in *CVPR*, 2020, pp. 7191–7201.
- [21] Marius Leordeanu and Martial Hebert, “A spectral technique for correspondence problems using pairwise constraints,” in *ICCV*, 2005, vol. 2, pp. 1482–1489.
- [22] Zhi Chen, Kun Sun, Fan Yang, and Wenbing Tao, “Sc2-ppcr: A second order spatial compatibility for efficient and robust point cloud registration,” in *CVPR*, 2022, pp. 13221–13231.
- [23] Xiyu Zhang, Jiaqi Yang, Shikun Zhang, and Yanning Zhang, “3d registration with maximal cliques,” in *CVPR*, 2023, pp. 17745–17754.
- [24] Kwang Moo Yi, Eduard Trulls, Yuki Ono, Vincent Lepetit, Mathieu Salzmann, and Pascal Fua, “Learning to find good correspondences,” in *CVPR*, 2018, pp. 2666–2674.
- [25] Charles Ruizhongtai Qi, Li Yi, Hao Su, and Leonidas J Guibas, “Pointnet++: Deep hierarchical feature learning on point sets in a metric space,” *NeurIPS*, vol. 30, 2017.
- [26] Jiaming Sun, Zehong Shen, Yuang Wang, Hujun Bao, and Xiaowei Zhou, “Loft: Detector-free local feature matching with transformers,” in *CVPR*, 2021, pp. 8922–8931.
- [27] Philipp Lindenberger, Paul-Edouard Sarlin, and Marc Pollefeys, “Lightglue: Local feature matching at light speed,” in *ICCV*, 2023.
- [28] Aleksandr Segal, Dirk Haehnel, and Sebastian Thrun, “Generalized-icp,” in *Robotics: science and systems*, 2009, vol. 2, p. 435.
- [29] Hao Yu, Fu Li, Mahdi Saleh, Benjamin Busam, and Slobodan Ilic, “Cofinet: Reliable coarse-to-fine correspondences for robust pointcloud registration,” *NeurIPS*, vol. 34, pp. 23872–23884, 2021.
- [30] Guiyu Zhao, Zhentao Guo, Xin Wang, and Hongbin Ma, “Spherenet: Learning a noise-robust and general descriptor for point cloud registration,” *IEEE Trans. Geosci. Remote Sens.*, pp. 1–1, 2023.
- [31] Hao Yu, Zheng Qin, Ji Hou, Mahdi Saleh, Dongsheng Li, Benjamin Busam, and Slobodan Ilic, “Rotation-invariant transformer for point cloud matching,” in *CVPR*, 2023, pp. 5384–5393.
- [32] Zan Gojcic, Caifa Zhou, Jan D Wegner, and Andreas Wieser, “The perfect match: 3d point cloud matching with smoothed densities,” in *CVPR*, 2019, pp. 5545–5554.

A. IMPLEMENTATION DETAILS

Our approach is implemented using PyTorch and Open3D. We conducted two distinct preprocesses on the 3DMatch dataset to generate training sets for both the homologous registration model and the cross-source registration model. For homologous registration, following [4], we downsample the point cloud data using 0.02m voxels. To simulate density inconsistency in cross-source point cloud data for cross-source registration, we further processed 3DMatch. The source and target point clouds underwent data augmentation through random voxel downsampling, with voxel side lengths following a uniform distribution $U(0, 0.1)$ (it’s worth noting that the voxel side lengths for the source and target point clouds are uncorrelated). During training, we utilize a batch size of 64, and the initial learning rate is set to 0.001, reducing by 50% every 5 epochs. All experiments reported in this paper are conducted on a single Nvidia RTX 3090 with 24GB memory.

B. DETAILED METRICS

Following [7], we utilize Translation Error (TE), Rotation Error (RE), and Registration Recall (RR) to evaluate our method. Additionally, Following [2], we assess correspondence results using Inlier Ratio (IR) and Feature Matching Recall (FMR). (1) RE: the geodesic distance between the ground-truth and the estimated rotation matrix. (2) TE: the Euclidean distance between the ground-truth and the estimated translation vector. (3) RR: the proportion of registered successfully point cloud pairs ($RE < 15^\circ$ and $TE < 30\text{cm}$) to the total point cloud pairs in the dataset. (4) IR: the proportion of estimated correct correspondences ($< 0.1\text{m}$) to the total ground-truth correspondences. (5) FMR: the proportion of point clouds with successful feature matching ($IR > 0.05$) to the total point cloud pairs in the dataset.

Inlier Ratio (IR) is the proportion of estimated correct correspondences ($< 0.1\text{m}$) to the total ground-truth correspondences:

$$IR_h = \frac{1}{|\mathcal{G}_h|} \sum_{(\mathbf{p}_i, \mathbf{q}_j) \in \mathcal{G}_h} \mathbb{1}(\|\mathbf{T}_h(\mathbf{p}_i) - \mathbf{q}_j\|_2 < \tau_1) \quad (11)$$

where \mathcal{G}_h is the correspondences of the h^{th} point cloud pair in the test dataset and $\mathbb{1}$ is an indicator function. $\mathbf{T}(\mathbf{p}_i)$ is the point after transformation \mathbf{T} from \mathbf{p}_i .

Feature Matching Recall (FMR) represents the proportion of point clouds with successful feature matching ($IR_h > 0.05$) to the total point cloud pairs in the dataset

$$FMR = \frac{1}{H} \sum_{h=1}^H \mathbb{1}(IR_h > \tau_2) \quad (12)$$

where H is the number of point cloud pairs in the dataset.

Rotation Error (RE) represents the geodesic distance between the ground-truth rotation matrix \mathbf{R}_h and the estimated rotation matrix $\hat{\mathbf{R}}_h$:

$$RE_h = \arccos\left(\frac{\text{trace}(\hat{\mathbf{R}}_h^T \mathbf{R}_h) - 1}{2}\right) \quad (13)$$

Translation Error (TE) represents the Euclidean distance between the ground-truth translation vector \mathbf{t} : and the estimated translation vector $\hat{\mathbf{t}}_h$:

$$TE_h = \|\hat{\mathbf{t}}_h - \mathbf{t}_h\| \quad (14)$$

Registration Recall (RR) Following [7, 6], for cross-source registration, $RE_h < 15^\circ$ and $TE_h < 30\text{cm}$ is considered as successful registration. Therefore, RR in the cross-source point cloud registration can be calculated as:

$$RR = \frac{1}{H} \sum_{h=1}^H \mathbb{1}(TE_h < 0.3 \text{ m} \wedge RE_h < 15^\circ) \quad (15)$$

C. MORE EXPERIMENTAL RESULTS

C.1. More qualitative results

In this section, we present additional visualization experiments and qualitative results. As illustrated in Figure 5 and 6, our method demonstrates robust and accurate registration with low RE and TE. Moreover, owing to our hierarchical correspondence filtering, our method obtains high-quality correspondences.

C.2. Runtime analysis

Method	Kinect_sfm			Kinect_lidar		
	Feature (s) ↓	Pose (s) ↓	Total (s) ↓	Feature (s) ↓	Pose (s) ↓	Total (s) ↓
ICP [9]	-	<u>0.83</u>	<u>0.83</u>	-	4.03	4.03
RANSAC [11]	41.9	-	-	4.10	0.14	-
GCC [7]	-	2.98	2.98	-	<u>4.21</u>	<u>4.21</u>
Predator [4]	0.10	0.18	0.28	0.68	0.25	0.93
CoFiNet [29]	0.31	0.28	0.59	0.19	0.22	0.41
GeoTrans [2]	0.07	0.06	0.13	0.09	<u>0.14</u>	0.23
Perfectmatch [32]	76.31	0.88	77.19	108.90	0.97	109.87
SpinNet [3]	106.29	1.50	107.79	159.49	1.16	160.65
VRHCF (ours)	<u>8.27</u>	<u>0.10</u>	<u>8.32</u>	<u>8.38</u>	0.12	<u>8.60</u>

Table 4. Runtime analysis on 3DCSR.

We conduct experiments to assess the running time, and the results are presented in Table 4. The first three in Table 4 are traditional algorithms, the middle three are fragment-based methods, and the last three are patch-based methods. Although our method belonging to patch-based methods is far inferior to fragment-based methods in speed, our method exhibits the best performance in runtime efficiency compared with other patch-based methods [3, 32]. Regarding feature extraction, although we choose the time-consuming

3DCCN backbone for the consideration of generalization performance, we abandon the point layer and replace it with simple and efficient spherical voxelization, which greatly reduces the time consumption of our feature extraction. In solving the pose, although we use multi-layer correspondence filtering, it only performs Topk selection based on the consistency score. Finally, we use SVD to solve the pose, which is much faster than RANSAC.

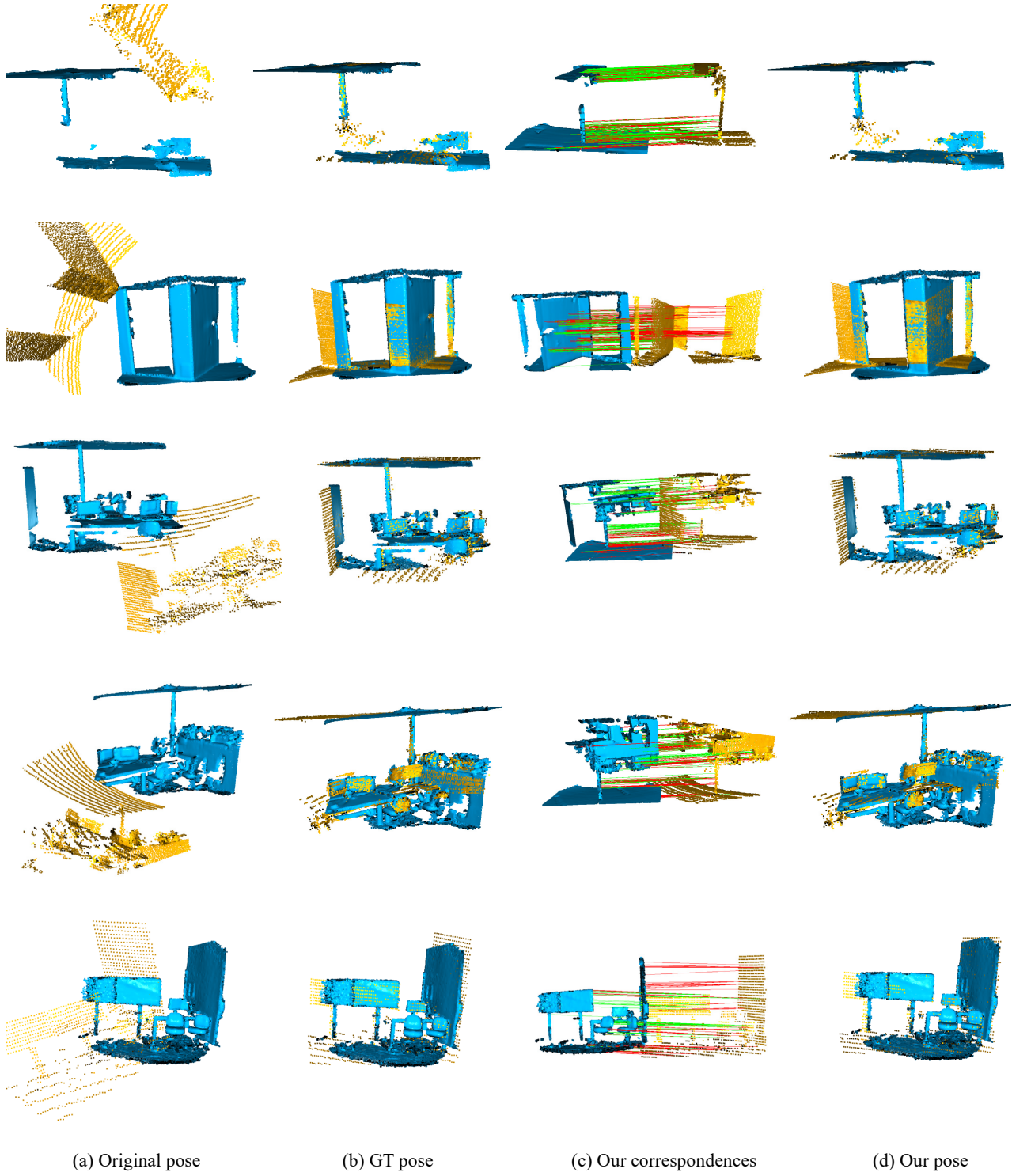
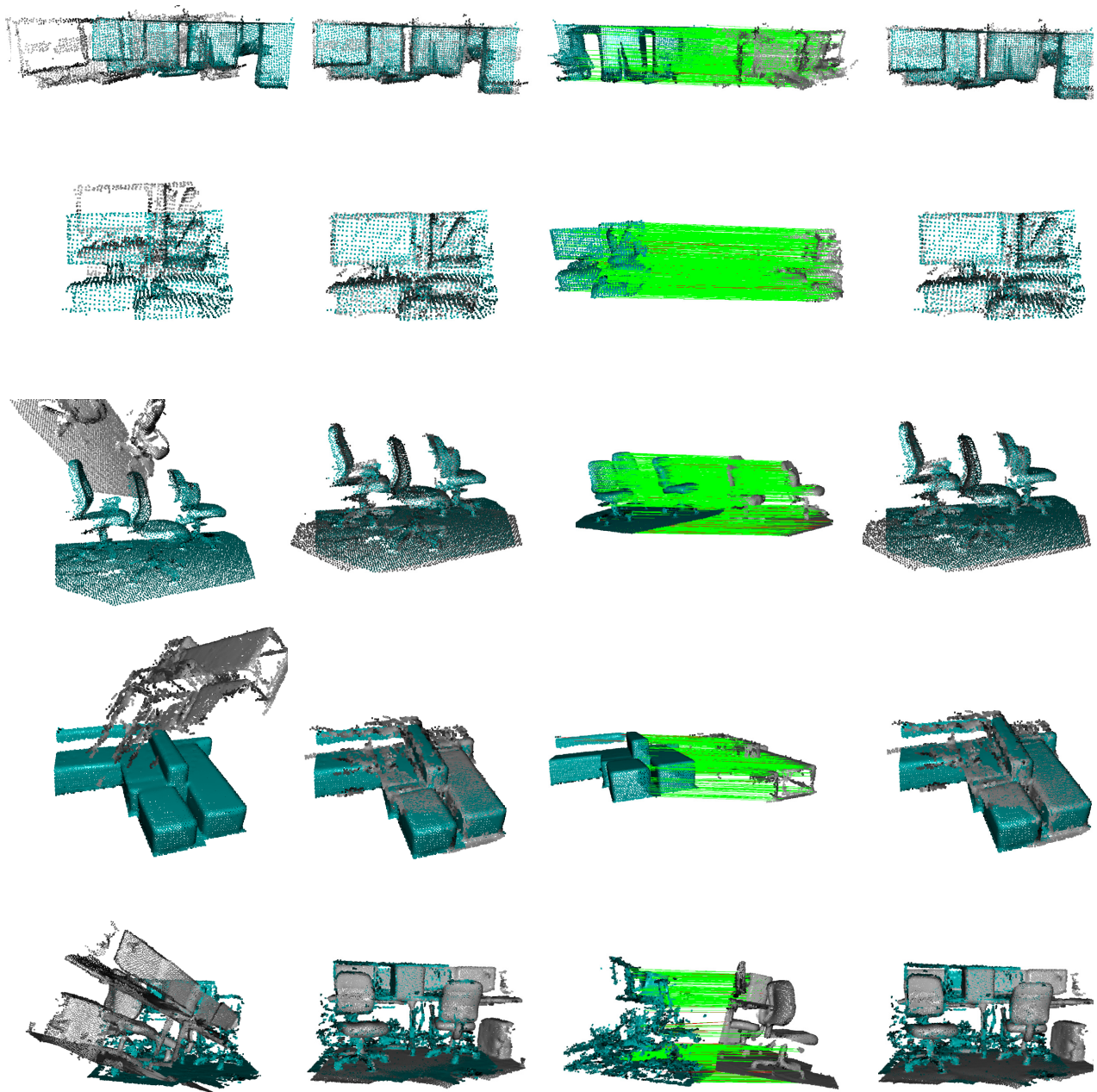


Fig. 5. qualitative results on Kinect-SFM.



(a) Original pose

(b) GT pose

(c) Our correspondences

(d) Our pose

Fig. 6. qualitative results on Kinect-SFM.